Algorithms for remote estimation of chlorophyll-a in coastal and inland waters using red and near infrared bands

Alexander A. Gilerson,[1,*] Anatoly A. Gitelson,[2] Jing Zhou,[1] Daniela Gurlin,[2] Wesley Moses,[2] Ioannis Ioannou,[1] and Samir A. Ahmed[1]

[1]*Optical Remote Sensing Laboratory, Department of Electrical Engineering, The City College of the City University of New York, 140 St & Convent Ave, New York, New York 10031 USA*

[2]*Center for Advanced Land Management Information Technologies (CALMIT), School of Natural Resources, University of Nebraska-Lincoln, USA*

**gilerson@ccny.cuny.edu*

Abstract: Remote sensing algorithms that use red and NIR bands for the estimation of chlorophyll-a concentration [Chl] can be more effective in inland and coastal waters than algorithms that use blue and green bands. We tested such two-band and three-band red-NIR algorithms using comprehensive synthetic data sets of reflectance spectra and inherent optical properties related to various water parameters and a very consistent *in situ* data set from several lakes in Nebraska, USA. The two-band algorithms tested with MERIS bands were $R_{rs}(708)/R_{rs}(665)$ and $R_{rs}(753)/R_{rs}(665)$. The three-band algorithm with MERIS bands was in the form $R3 = [R_{rs}^{-1}(665) - R_{rs}^{-1}(708)] \times R_{rs}(753)$. It is shown that the relationships of both $R_{rs}(708)/R_{rs}(665)$ and R3 with [Chl] do not depend much on the absorption by CDOM and non-algal particles, or the backscattering properties of water constituents, and can be defined in terms of water absorption coefficients at the respective bands as well as the phytoplankton specific absorption coefficient at 665 nm. The relationship of the latter with [Chl] was established for [Chl] > 1 mg/m^3 and then further used to develop algorithms which showed a very good match with field data and should not require regional tuning.

OCIS codes: (010.4450) Ocean optics; (280.0280) Remote sensing.

References and links

1. G. Moore, J. Aiken, and J. Lavender, "The atmospheric correction of water colour and the quantitative retrieval of suspended particulate matter in Case II waters: application to MERIS," Int. J. Remote Sens. **20**(9), 1713–1733 (1999).
2. J. Aiken, and G. Moore, "ATBD case 2 bright pixel atmospheric correction," Center for Coastal & Marine Sciences, Plymouth Marine Laboratory, U.K., Rep, PO-TN-MEL-GS **4**, 0005 (2000).
3. M. Wang, and W. Shi, "Estimation of ocean contribution at the MODIS near-infrared wavelengths along the east coast of the U.S.: Two case studies," Geophys. Res. Lett. **32**(13), L13606 (2005), doi:10.1029/2005GL022917.
4. M. Wang, and W. Shi, "The NIR-SWIR combined atmospheric correction approach for MODIS ocean color data processing," Opt. Express **15**(24), 15722–15733 (2007).
5. R. Doerffer, and H. Schiller, "MERIS regional coastal and lake case 2 water project atmospheric correction ATBD," Institute for Coastal Research, GKSS Research Center, Geesthacht, Germany, Rep, GKSS-KOF-MERIS-ATB **D01**, 1 (2008).
6. P. J. Werdell, S. W. Bailey, B. A. Franz, L. W. Harding, Jr., G. C. Feldman, and C. R. McClain, "Regional and seasonal variability of chlorophyll-a in Chesapeake Bay as observed by SeaWiFS and MODIS-Aqua," Remote Sens. Environ. **113**(6), 1319–1330 (2009).
7. A. A. Gitelson, G. Keydan, and V. Shishkin, "Inland waters quality assessment from satellite data in visible range of the spectrum," Sov. Remote Sens. **6**, 28–36 (1985).

#134029 - $15.00 USD Received 25 Aug 2010; revised 25 Oct 2010; accepted 26 Oct 2010; published 3 Nov 2010

8. R. P. Stumpf, and M. A. Tyler, “Satellite detection of bloom and pigment distributions in estuaries,” Remote Sens. Environ. **24**(3), 385–404 (1988).
9. A. A. Gitelson, “The peak near 700 nm on radiance spectra of algae and water: relationships of its magnitude and position with chlorophyll concentration,” Int. J. Remote Sens. **13**(17), 3367–3373 (1992).
10. A. A. Gitelson, G. Dall’Olmo, W. Moses, D. C. Rundquist, T. Barrow, T. R. Fisher, D. Gurlin, and J. Holz, “A simple semi-analytical model for remote estimation of chlorophyll-a in turbid waters: Validation,” Remote Sens. Environ. **112**(9), 3582–3593 (2008).
11. H. R. Gordon, “Diffuse reflectance of the ocean: the theory of its augmentation by chlorophyll a fluorescence at 685 nm,” Appl. Opt. **18**(8), 1161–1166 (1979).
12. A. Vasilkov, and O. Kopelevich, “Reasons for the appearance of the maximum near 700 nm in the radiance spectrum emitted by the ocean layer,” Oceanology (Mosc.) **22**, 697–701 (1982).
13. J. F. Schalles, “Optical Remote Sensing Techniques to Estimate Phytoplankton Chlorophyll a Concentrations in Coastal Waters with Varying Suspended Matter and CDOM Concentrations,” in Remote Sensing of Aquatic Coastal Ecosystem Processes: Science and Management Applications, L.L. Richardson and E.F. LeDrew, eds. (Springer, 2006), Chap. 3.
14. G. Dall'Olmo, A. A. Gitelson, and D. C. Rundquist, “Towards a unified approach for remote estimation of chlorophyll-a in both terrestrial vegetation and turbid productive waters,” Geophys. Res. Lett. **30**(18), 1938 (2003), doi:10.1029/2003GL018065.
15. L. Han, and D. Rundquist, “Comparison of NIR/Red ratio and first derivative of reflectance in estimating algal-chlorophyll concentration: a case study in a turbid reservoir,” Remote Sens. Environ. **62**(3), 253–261 (1997).
16. C. Le, Y. Li, Y. Zha, D. Sun, C. Huang, and H. Lu, “A four-band semi-analytical model for estimating chlorophyll a in highly turbid lakes: The case of Taihu Lake, China,” Remote Sens. Environ. **113**(6), 1175–1182 (2009).
17. H. J. Gons, M. Rijkeboer, and K. G. Ruddick, “A chlorophyll-retrieval algorithm for satellite imagery (Medium Resolution Imaging Spectrometer) of inland and coastal waters,” J. Plankton Res. **24**(9), 947–951 (2002).
18. K. G. Ruddick, H. J. Gons, M. Rijkeboer, and G. Tilstone, “Optical remote sensing of chlorophyll a in case 2 waters by use of an adaptive two-band algorithm with optimal error properties,” Appl. Opt. **40**(21), 3575–3585 (2001).
19. J. Gower, S. King, G. Borstad, and L. Brown, “Detection of intense plankton blooms using the 709 nm band of the MERIS imaging spectrometer,” Int. J. Remote Sens. **26**(9), 2005–2012 (2005).
20. G. Dall’Olmo, and A. A. Gitelson, “Effect of bio-optical parameter variability on the remote estimation of chlorophyll-a concentration in turbid productive waters: experimental results,” Appl. Opt. **44**(3), 412–422 (2005).
21. A. A. Gitelson, J. Schalles, and C. M. Hladik, “Remote chlorophyll-a retrieval in turbid productive estuarine: Chesapeake Bay case study,” Remote Sens. Environ. **109**(4), 464–472 (2007).
22. G. Dall’Olmo, and A. A. Gitelson, “Effect of bio-optical parameter variability and uncertainties in reflectance measurements on the remote estimation of chlorophyll-a concentration in turbid productive waters: modeling results,” Appl. Opt. **45**(15), 3577–3592 (2006).
23. C. D. Mobley, *Light and Water. Radiative Transfer in Natural Waters* (Academic Press, New York, 1994).
24. A. Gilerson, J. Zhou, S. Hlaing, I. Ioannou, J. Schalles, B. Gross, F. Moshary, and S. Ahmed, “Fluorescence component in the reflectance spectra from coastal waters. Dependence on water composition,” Opt. Express **15**(24), 15702–15721 (2007).
25. Z. P. Lee, http://www.ioccg.org/groups/OCAG_data.html.
26. A. M. Ciotti, M. R. Lewis, and J. J. Cullen, “Assessment of the relationships between dominant cell size in natural phytoplankton communities and the spectral shape of the absorption coefficient,” Limnol. Oceanogr. **47**(2), 404–417 (2002).
27. A. Bricaud, M. Babin, A. Morel, and H. Claustre, “Variability in the chlorophyll-specific absorption coefficients of natural phytoplankton: Analysis and parameterization,” J. Geophys. Res. **100**(C7), 13321–13332 (1995).
28. A. A. Gitelson, D. Gurlin, W. J. Moses, and T. Barrow, “A bio-optical algorithm for the remote estimation of the chlorophyll-a concentration in case 2 waters,” Environ. Res. Lett. **4**(4), 045003 (2009), doi:10.1088/1748-9326/4/4/045003.
29. W. J. Moses, A. A. Gitelson, S. Berdnikov, and V. Povazhnyy, “Satellite Estimation of Chlorophyll-a Concentration Using the Red and NIR Bands of MERIS—The Azov Sea Case Study,” IEEE Geosci. Remote Sens. Lett. **6**(4), 845–849 (2009).
30. H. R. Gordon, O. B. Brown, R. H. Evans, J. W. Brown, R. C. Smith, K. S. Baker, and D. K. Clark, “A semianalytic radiance model of ocean color,” J. Geophys. Res. **93**(D9), 10909–10924 (1988).
31. R. C. Smith, and K. S. Baker, “Optical properties of the clearest natural waters (200-800 nm),” Appl. Opt. **20**(2), 177–184 (1981).
32. J. Zhou, A. Gilerson, I. Ioannou, S. Hlaing, J. Schalles, B. Gross, F. Moshary, and S. Ahmed, “Retrieving quantum yield of sun-induced chlorophyll fluorescence near surface from hyperspectral in-situ measurement in productive water,” Opt. Express **16**(22), 17468–17483 (2008).
33. P. Gege, and A. Albert, “A tool for inverse modeling of spectral measurements in deep and shallow waters,” in Remote Sensing of Aquatic Coastal Ecosystem Processes: Science and Management Applications, L.L. Richardson and E.F. LeDrew, eds. Chap. 4, Springer, 2006.

#134029 - $15.00 USD Received 25 Aug 2010; revised 25 Oct 2010; accepted 26 Oct 2010; published 3 Nov 2010

34. J. E. O'Reilly, and 24 Coauthors, "SeaWiFS Postlaunch Calibration and Validation Analyses, Part 3," in NASA Tech. Memo. 2000–206892, Vol. 11, S. B. Hooker and E. R. Firestone, eds., (NASA Goddard Space Flight Center, Greenbelt, MD, 2000) 49 pp.

1. Introduction

Recent advances in the development of atmospheric correction models [1–5] have made the retrieval of reflectance of coastal and inland waters from electromagnetic signals from the top of the atmosphere more accurate and have inspired further development of retrieval algorithms for turbid productive waters and their analysis [6]. This includes algorithms that employ wavebands in the red and near infrared (NIR) range (650-800 nm), which are less sensitive than traditional blue-green (440-550 nm) ratio algorithms to the absorption by colored dissolved organic matter (CDOM) and scattering by mineral particles: both CDOM absorption and particulate scattering decrease rapidly with the wavelength and are small in the red-NIR part of the spectrum. Simple red-NIR band ratio algorithms have been known for a long time [7–9] and successfully used for the estimation of chlorophyll-*a* concentration [Chl] from reflectance spectra in coastal and inland waters [10] for [Chl] above 3-5 mg/m^3 when the reflectance peak around 700 nm [9] becomes quite pronounced. Generally this peak includes two components: i) an elastic component which corresponds to the local minimum of absorption coefficient due to the confluence of the phytoplankton and water absorption spectra, and ii) chlorophyll fluorescence with a maximum near 685 nm [9,11,12]. For [Chl] < 3-5 mg/m^3, the elastic component of the peak is small and the magnitude of the peak above the baseline is mostly related to the chlorophyll fluorescence signal. For [Chl] > 3-5 mg/m^3, both components contribute to the signal, with the peak of the elastic component and the resulting combined reflectance moving towards longer wavelengths and the minimum in reflectance, which is due to the phytoplankton absorption peak around 675 nm, becoming more pronounced, as [Chl] increases.

Many algorithms have been developed which employ two or more bands in the red-NIR spectral range or use a combination of these bands with bands in the blue-green part of the spectrum (see the comprehensive review in [13] and other references [14–16]). Some of the algorithms included correction for the backscattering at different bands [17] and the band tuning procedures [18]. In most cases, the algorithms had spectral bands where the contribution of chlorophyll fluorescence cannot be considered negligible. Such algorithms required additional tuning and often did not produce acceptable accuracies in retrieving [Chl], especially for [Chl] values below 10 mg/m^3. Moreover, the bands in some of the algorithms are not available on the current ocean color satellites, which limits the applicability of those algorithms. Gower [19] introduced the Maximum Chlorophyll Index (MCI), which was successfully used for the detection of algal blooms. This index uses bands at 681, 709 and 753 nm, so it is very sensitive to the chlorophyll fluorescence and is used only for qualitative detection of algal blooms.

The advanced version of red-NIR algorithm [10] includes three bands instead of two [14], which enables better separation of the absorption by [Chl] from absorption and scattering by other constituents in water in the red and NIR parts of the spectrum. Both two- and three-band algorithms have been tested in multiple water environments [10,20,21]. But the sources of the uncertainties were difficult to trace because multiple parameters involved (absorption and backscattering coefficients of water components) were not directly measured in the experiments. Optimization of the band positions was done using the synthetic data sets simulated with a semi-analytical model [22]. However, the sensitivity of the retrievals to CDOM absorption, concentration of minerals, and shape of phytoplankton absorption spectrum were not considered.

In this work we tested two- and three-band algorithms with bands that matched the spectral channels of MERIS (Medium Resolution Imaging Spectrometer) centered at 665, 708 and 753 nm. Comprehensive synthetic data sets of reflectance spectra and inherent optical

#134029 - $15.00 USD Received 25 Aug 2010; revised 25 Oct 2010; accepted 26 Oct 2010; published 3 Nov 2010

properties (IOP) for a wide range of water constituents were used together with field data. Specifically, we analyzed relationships between [Chl] and $R_{rs}(708)/R_{rs}(665)$, $R_{rs}(753)/R_{rs}(665)$, and $[R_{rs}(665)^{-1} - R_{rs}(708)^{-1}]*R_{rs}(753)$, where $R_{rs}(\lambda)$ is the remote sensing reflectance at the wavelengths λ = 665, 708, and 753 nm. The main goal of the work was to analyze the contributions of different components to the estimated [Chl] values and arrive at more robust algorithms which would not require significant regional tuning.

In Section 2, which follows, we describe our methods, which are based on our synthetic and field (*in situ)* data sets; in Sections 3-6 we report results, specifically, in Section 3 we make a preliminary analysis of the sensitivity of the algorithms to water quality parameters; in Section 4 we analyze the contributions of main components to the relationships between the algorithms and [Chl]; in Section 5 we establish the relationship between the phytoplankton specific absorption coefficient in the red-NIR part of the spectrum and [Chl]; in Section 6 we arrive at more accurate algorithms that relate [Chl] and reflectances; and in Section 7 we analyze the performance of blue-green ratio algorithms on the same data sets and compare them with the performance of the red-NIR algorithms.

2. Description of the data sets

About two thousand reflectance spectra were simulated using Hydrolight [23], with and without taking into account the chlorophyll fluorescence, with 1 nm resolution for a wide range of conditions typical for inland and coastal waters: [Chl] = 1-100 mg/m^3, CDOM (yellow substance) absorption coefficient at 400 nm, $a_y(400)$ = 0-5 m^{-1}, different shapes of phytoplankton specific absorption coefficient spectra, and concentrations of non-algal particles, C_{NAP} = 0-10 mg/l. All the details and assumptions used for the simulation of water optical properties are given in Gilerson et al. [24]. They were based on the findings of many authors for IOP characteristics, with similar assumptions to those used in the development of the data sets of the IOCCG working group [25], and included variations of absorption and backscattering spectra in a very wide range [24]. Thus, for example, the power coefficient in the CDOM absorption model, $a_y = a_y(400)*\exp[-S_y(\lambda - 400)]$, was in the range S_y = 0.1-0.2 nm^{-1} and the specific scattering of non-algal particles, b^*_{NAP}, was in the range 0.5-1.0 m^2/g. Solar input was simulated with a cloud-free sky.

To be able to analyze the impact of the phytoplankton specific absorption coefficient, a^*_{ph}, on the performance of the algorithms, as a first step, two data sets were simulated with the shapes of the specific absorption coefficient spectra taken, according to Eq. (2) from Ciotti et al. [26], as a sum of the specific absorptions coefficients of microplankton and picoplankton, as shown in Fig. 1. The weighting factor S_f ranged from 0.1 to 0.3. C_{NAP} ranged from 0 to 1 mg/l in one data set and from 1 to 10 mg/l in the other data set. It should be noted that based on the dependence of a^*_{ph} (440) on [Chl], as shown in [27], the range 0-0.3 for S_f is typical for [Chl] > 1mg/m^3. But we found that the model [26] usually underestimates a^*_{ph} values in the red and NIR parts of the spectrum [see Fig. 8(b) below]. For the purpose of evaluating the red–NIR models, we also used the spectral shapes from the model [26] in the 650-800 nm part of the spectrum with $a^*_{ph}(675)$ = 0.0142, 0.0156, and 0.02 m^2/(mg Chl a) which are also shown in Fig. 1. For the spectral shapes with $a^*_{ph}(675)$ = 0.0142 and 0.02 m^2(mg Chl a)$^{-1}$ an additional set of IOP spectra and the associated reflectances was generated with C_{NAP} = 0-10 mg/l, 1 < [Chl] < 40 mg/m^3 (1 < [Chl] < 20 mg/m^3 for $a^*_{ph}(675)$ = 0.02 m^2/(mg Chl a) and CDOM absorption at 400 nm, $a_y(400)$ = 0-3 m^{-1}. This range of [Chl], 1 < [Chl] < 40 mg/m^3, is more typical for coastal and inland waters (rather than higher [Chl] values). Thus, a very accurate evaluation of the algorithms is required for this [Chl] range. In all simulations the phytoplankton absorption was considered proportional to [Chl]

#134029 - $15.00 USD Received 25 Aug 2010; revised 25 Oct 2010; accepted 26 Oct 2010; published 3 Nov 2010

$$a_{ph}(\lambda) = [Chl]a^*_{ph}(\lambda) \quad (1)$$

and

$$a^*_{ph}(\lambda) = S_f \cdot a^*_{pico}(\lambda) + (1 - S_f) \cdot a^*_{micro}(\lambda) \quad (2)$$

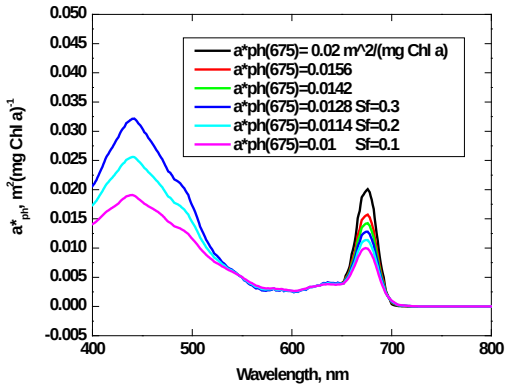

Fig. 1. Phytoplankton specific absorption spectra used in the simulations.

Fluorescence quantum yield (together with the chlorophyll reabsorption coefficient) in the original simulations for S_f = 0.1-0.3 was, η = 0.5%. The fluorescence contribution was calculated as the difference between the total and elastic reflectances and was assumed to change proportionally with η, which enabled the assessment of the impact of the fluorescence component. All reflectances were simulated for the sun zenith angle θ_i = 30° and for nadir viewing.

Field data set consisted of data collected by the CALMIT group at 85 stations in Fremont State Lakes, Nebraska, USA, during the summer of 2008, with [Chl] = 2-100 mg/m^3, $a_y(400)$ = 0.9-3 m^{-1}, and C_{NAP} = 0-3 mg/l [28]. A standard set of water quality parameters was measured: turbidity, [Chl], total, inorganic, and organic suspended solids. Hyperspectral reflectance measurements were taken from a boat using two intercalibrated Ocean Optics USB2000 spectrometers. More details on the instrumentation and methodology are provided in Gitelson et al [28].

3. Preliminary analysis of the main factors impacting red – NIR algorithms

3.1 Comparison of the synthetic and field data

Moses et al. [29] calibrated and validated red-NIR models using MERIS satellite reflectances and [Chl] measured in the field. As a result of the calibration, the following linear relationships between [Chl] and the models were obtained.

The two-band MERIS algorithm:

$$[\text{Chl}] = 61.324 * R_{rs}(708) / R_{rs}(665) - 37.94 \quad (3)$$

The three-band MERIS algorithm:

$$[\text{Chl}] = 232.329[(R_{rs}(665)^{-1} - R_{rs}(708)^{-1}) * R_{rs}(753)] + 23.174 \quad (4)$$

These relationships are compared in Fig. 2 with the relationships obtained between the models and [Chl] simulated from the synthetic data set for $a^*_{ph}(675)$ = 0.0156 m^2/(mg Chl a). As can be seen, for both two-band and three-band models, the relationships obtained from the

#134029 - $15.00 USD Received 25 Aug 2010; revised 25 Oct 2010; accepted 26 Oct 2010; published 3 Nov 2010

synthetic data set are closely related to those obtained from the field data set (RMSE = 4.05 mg/m^3 and 5.58 mg/m^3, respectively). Although further detailed analysis is required, especially for low [Chl] values, the close similarity of these relationships prompted the study of the sensitivity of the algorithms to variable water parameters.

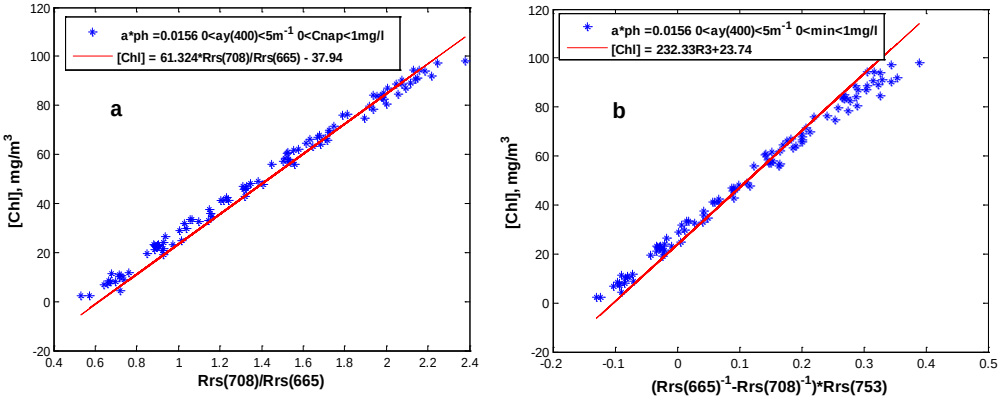

Fig. 2. Comparison of estimates of chlorophyll-a concentrations calculated using Eq. (3) (a) and Eq. (4) (b) and by synthetic reflectance spectra with $a^*_{ph}(675)$ = 0.0156 m^2/(mg Chl a) (blue dots): a) two-band algorithm, b) three-band algorithm.

For all simulations from the synthetic data, remote sensing reflectances, R_{rs}, at the band centers were used instead of integrating the water leaving radiance over the entire bandwidth and normalizing it by the irradiance over the same spectral range. This was done because the latter approach did not produce a noticeable change in the performance of the algorithms.

3.2 Sensitivity of the two-band model to water parameters

The two-band model, $R_{rs}(708)/R_{rs}(665)$, was further analyzed using synthetic data sets. The impact of a^*_{ph} on the relationship between the model values and [Chl] is shown in Fig. 3. In Fig. 3, $a^*_{ph}(675)$ is in the range 0.01-0.156 m^2/(mg Chl a); CDOM absorption is in the range, $0 < a_y(400) < 5\text{m}^{-1}$; C_{NAP} is in the range, $0 < C_{NAP} < 1$mg/l. It can be seen that the relationship between [Chl] and $R_{rs}(708)/R_{rs}(665)$ is sensitive to a^*_{ph} values. However, not all this variability can be seen for the realistic concentrations of water constituents: it is well known that due to the packaging effect [27] the values of a^*_{ph} in all parts of the spectrum as well as the variability of a^*_{ph} decreases with increasing [Chl]. So the actual sensitivity of the model to a^*_{ph} should be assessed by taking into account the relationship between [Chl] and a^*_{ph}.

#134029 - $15.00 USD Received 25 Aug 2010; revised 25 Oct 2010; accepted 26 Oct 2010; published 3 Nov 2010

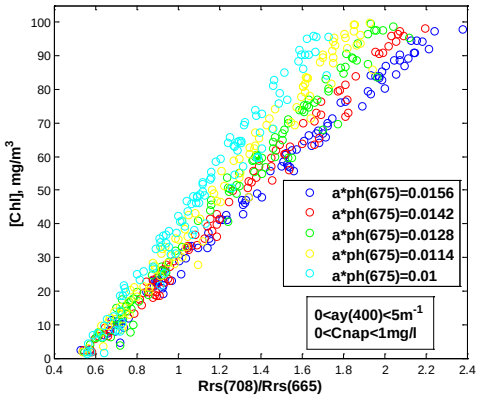

Fig. 3. Chlorophyll-a concentration vs. two-band red-NIR model calculated using synthetic data, the impact of the shape of the phytoplankton specific absorption coefficient.

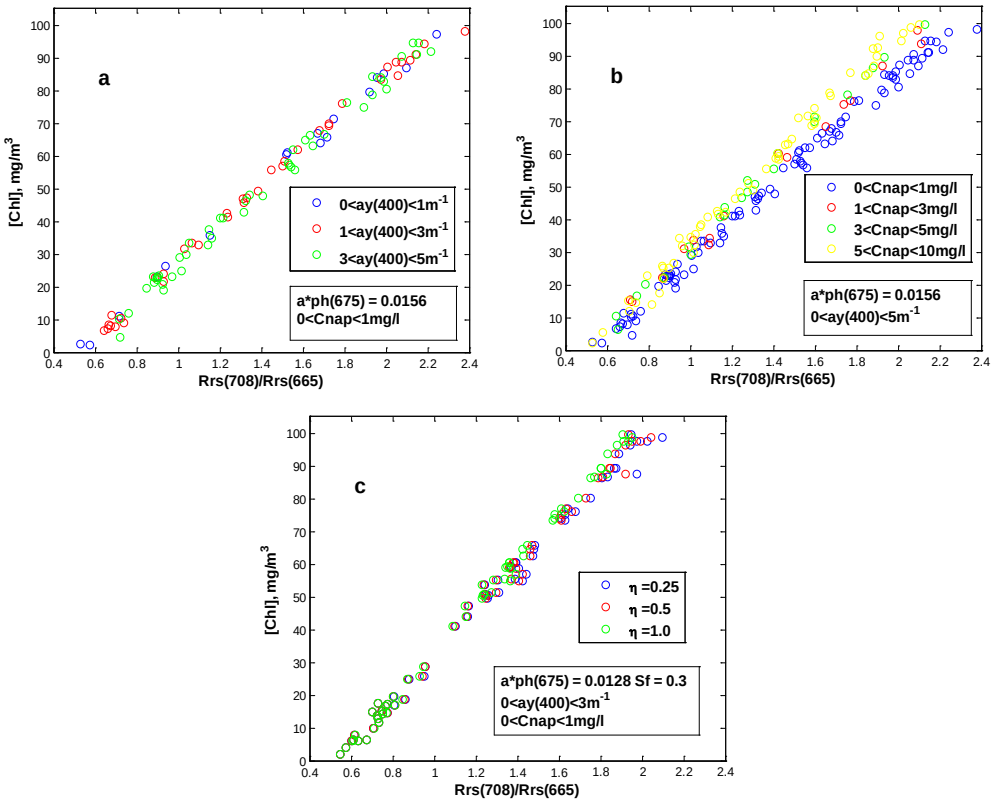

Fig. 4. Chlorophyll-a concentration vs. two-band red-NIR ratio with variations in (a) CDOM absorption, $0<a_y(400)<5m^{-1}$, (b) C_{NAP} concentration, $0<C_{NAP}<10$ mg/l, and (c) fluorescence quantum yield, $\eta = 0.25$, 0.5 and 1.0.

Sensitivity of the $R_{rs}(708)/R_{rs}$ (665) model to changes in CDOM absorption is presented in Fig. 4(a), which shows minimal impact for a very broad range of CDOM absorption coefficient values, $0 < a_y(400) < 5m^{-1}$. The impact of C_{NAP} variability is shown in Fig. 4(b): for a very wide variation in C_{NAP} values, $0 < C_{NAP} < 10$ mg/l, standard deviation was 4.58

#134029 - $15.00 USD Received 25 Aug 2010; revised 25 Oct 2010; accepted 26 Oct 2010; published 3 Nov 2010

mg/m^3, thereby showing that variations in C_{NAP} do not dramatically affect the accuracy of [Chl] estimation. Results of simulations for three values of fluorescence quantum yield, η = 0.25, 0.5, and 1.0, showed that small differences can be observed only for [Chl] > 60 mg/m^3 [Fig. 4(c)]. The impacts of a_{ph}^*, $a_y(400)$, C_{NAP}, and η were found to be similar for the three-band model and are not shown here.

Thus, the variability of a_{ph}^* and the relationship between [Chl] and a_{ph}^* are the major factors that affect the performance of the $R_{rs}(708)/R_{rs}(665)$ model. These factors should be assessed properly in order to make simulations that are relevant to realistic water conditions.

4. Basic relationships for red – NIR models and contributions from its main components

For inland and coastal waters the remote sensing reflectance can be estimated as [30]

$$R_{rs}(\lambda) = 0.53\frac{f}{Q}\frac{b_b(\lambda)}{a(\lambda)+b_b(\lambda)} \tag{5}$$

where $b_b(\lambda)$ is the backscattering coefficient, $a(\lambda)$ is the total absorption coefficient, f is a factor that depends mostly on the angle of the incident light, and Q is the bidirectional reflectance distribution function (BRDF) coefficient. Generally, both f and Q are also functions of the wavelength, but as a first order approximation, we ignore this dependence for the relatively narrow red – NIR spectral range of interest.

We also assume that the total absorption coefficient $a(\lambda)$ is the sum of absorption coefficients by four components: phytoplankton, CDOM, non-algal particles, and water

$$a(\lambda) = a_{ph}(\lambda) + a_y(\lambda) + a_{NAP}(\lambda) + a_w(\lambda) \tag{6}$$

Absorption by non-algal particles, $a_{NAP}(\lambda)$, has a spectral shape similar to that of the absorption by CDOM, and for the range of parameters considered, its magnitude was on average two times smaller than the CDOM absorption. To simplify the equations, $a_{NAP}(\lambda)$ is neglected henceforth in this model but this simplification will not in any way affect the analysis and the final results since $a_{NAP}(\lambda)$ was included in the bio-optical model for the calculation of the IOPs and the reflectances simulated using Hydrolight.

Thus, the ratio of the reflectances, which for two-band model we denote as R2, at two wavelengths λ_1 and λ_2 can be written as

$$\begin{aligned} R2 \;=\; & R_{rs}(\lambda_1)/R_{rs}(\lambda_2) = [b_b(\lambda_1)/b_b(\lambda_2)]*[a_{ph}(\lambda_2)+a_y(\lambda_2)+a_w(\lambda_2)+b_b(\lambda_2)]/ \\ & [a_{ph}(\lambda_1)+a_y(\lambda_1)+a_w(\lambda_1)+b_b(\lambda_1)] \end{aligned} \tag{7}$$

where, for our study, λ_1 = 708 or 753 nm and λ_2 = 665nm.

Assuming $[b_b(\lambda_1)/b_b(\lambda_2)] \approx 1$ (quite an accurate assumption for $R_{rs}(708)/R_{rs}(665)$ but less accurate for $R_{rs}(753/R_{rs}(665))$, we can find:

$$[a_{ph}(\lambda_1)+a_y(\lambda_1)+a_w(\lambda_1)+b_b(\lambda_1)]*R2 = [a_{ph}(\lambda_2)+a_y(\lambda_2)+a_w(\lambda_2)+b_b(\lambda_2)] \tag{8}$$

Taking into account (1) we arrive at a relationship similar to that in [17]

$$\begin{aligned} [\mathrm{Chl}] = & \{[a_y(\lambda_1)R2 - a_y(\lambda_2)] + [a_w(\lambda_1)R2 - a_w(\lambda_2)] + [b_b(\lambda_1)R2 - b_b(\lambda_2)]\}/ \\ & [a_{ph}^*(\lambda_2) - a_{ph}^*(\lambda_1)R2] \end{aligned} \tag{9}$$

#134029 - $15.00 USD Received 25 Aug 2010; revised 25 Oct 2010; accepted 26 Oct 2010; published 3 Nov 2010

Absorption coefficients of water at the wavelengths of interest are, $a_w(665) \approx 0.42$, $a_w(708) \approx 0.79$, and $a_w(753) \approx 2.5$ ([31] with interpolation). The range of R2 (see for example Fig. 2(a) for $R_{rs}(708)/R_{rs}(665)$ values) is R2 = 0.6-2.2. The differences between CDOM absorptions (i.e., $[a_y(\lambda_1)R2 - a_y(\lambda_2)]$), and backscatterings (i.e., $[b_b(\lambda_1)R2 - b_b(\lambda_2)]$), with R2 as a multiplier for the respective values at λ_1, are in the same form as the difference between water absorptions $[a_w(\lambda_1)R2 - a_w(\lambda_2)]$, with high values of $a_w(\lambda_1)$ and a significant difference between $a_w(\lambda_1)$ and $a_w(\lambda_2)$. So, for [Chl] > 5 mg/m^3, the contribution of CDOM absorption and backscattering terms are significantly smaller than the contribution from water absorption. At [Chl] < 5mg/m^3, when R2 < 0.6 and the water term becomes smaller, the variation in CDOM absorption and backscattering will create additional noise/uncertainties in the estimation of [Chl] values. The contributions of these components to the relationship [Chl] vs. $R_{rs}(708)/R_{rs}(665)$ is shown in Fig. 5. Simulations were done for the data set with $a_y(400)$ = 0-3 m^{-1} and C_{NAP} = 0-10 mg/l. In Fig. 5(a), $a^*_{ph}(675)$ = 0.0142 m^2/(mg Chl a) and [Chl] = 1-40 mg/m^3, and in Fig. 5(b), $a^*_{ph}(675)$ = 0.02 m^2/(mg Chl a) and [Chl] = 1-20 mg/m^3. It can be seen that the relationship is governed by the water absorption component with a small contribution from CDOM absorption and backscattering.

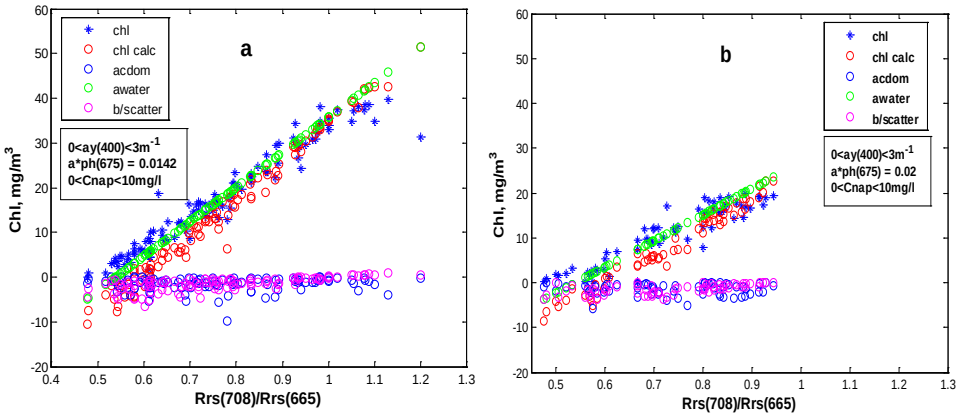

Fig. 5. Contributions of the main components of Eq. (9) to the relationship [Chl] vs. Rrs(708)/Rrs(665): The ranges of concentrations considered were, [Chl] = 1-40 mg/m^3, a_y = 0-3m^{-1}, C_{NAP} = 0-10 mg/l, for (a) $a^*_{ph}(675)$ = 0.0142 m^2/(mg Chl a) and (b) $a^*_{ph}(675)$ = 0.02 m^2/(mg Chl a). "chl" is the [Chl] from the synthetic data set, "chl calc" is the [Chl] calculated using the Eq. (9), "acdom" is $[a_y(\lambda_1)R2 - a_y(\lambda_2)]/a^*_{ph}(\lambda_2)$, the CDOM absorption term from Eq. (9), "awater" = $[a_w(\lambda_1)R2 - a_w(\lambda_2)]/a^*_{ph}(\lambda_2)$, the water absorption term from Eq. (9), and "b/scatter" is $[b_b(\lambda_1)R2 - b_b(\lambda_2)]/a^*_{ph}(\lambda_2)$, the backscattering term from Eq. (9).

There is no significant difference in the relationship between the cases of $a^*_{ph}(675)$ = 0.0142 m^2/(mg Chl a) [Fig. 5(a)] and $a^*_{ph}(675)$ = 0.02 m^2/(mg Chl a) [Fig. 5(b)]. $a^*_{ph}(\lambda_1)$ is very small, about 1% of $a^*_{ph}(\lambda_2)$, and it changes the slope of the relationship only slightly. There is also no significant scattering of points due to C_{NAP} variations.

For the [Chl] vs. $R_{rs}(753)/R_{rs}(665)$ relationship, the effect of different terms in Eq. (9), shown in Fig. 6, is completely different from those for the relationship [Chl] vs. $R_{rs}(708)/R_{rs}(665)$ shown in Fig. 5. The assumption $[b_b(\lambda_1)/b_b(\lambda_2)] \approx 1$ is not very accurate for the $R_{rs}(753)/R_{rs}(665)$ case. Thus, the water absorption term and "chl calc" [Eq. (9)] do not match the respective values simulated by Hydrolight. The contributions of CDOM absorption and backscattering terms from Eq. (9) are also significantly higher than those for the

#134029 - $15.00 USD Received 25 Aug 2010; revised 25 Oct 2010; accepted 26 Oct 2010; published 3 Nov 2010

$R_{rs}(708)/R_{rs}(665)$ model (Fig. 5), which makes the $R_{rs}(753)/R_{rs}(665)$ model unreliable for estimating low to moderate [Chl].

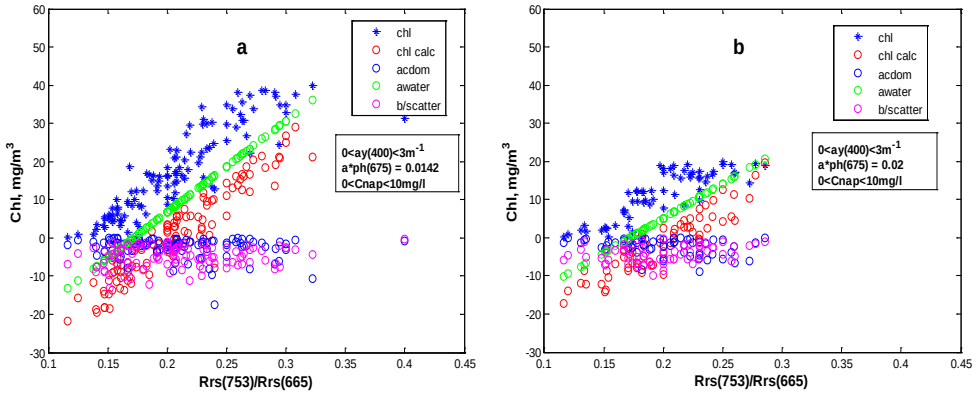

Fig. 6. Contributions of the main components of Eq. (9) to the relationship [Chl] vs. Rrs(753)/Rrs(665): a) $a^*_{ph}(675) = 0.0142$ m^2/(mg Chl a), b) $a^*_{ph}(675) = 0.02$ m^2/(mg Chl a). Notation and the ranges of values for [Chl], a_y, and C_{NAP} are the same as for Fig. 5.

Basic relationships for the three-band model, similar to the ones for the two-band model, can be written as follows: let us denote three-band model as

$$R3 = [Rrs(\lambda_1)^{-1} - Rrs(\lambda_2)^{-1}] * Rrs(\lambda_3) \quad (10)$$

where λ_1 = 665nm, λ_2 = 708nm and λ_3 = 753nm.

Then using Eqs. (5) and (6) we have

$$R3 = \{[a_{ph}(\lambda_1) + a_y(\lambda_1) + a_w(\lambda_1) + b_b(\lambda_1)]/b_b(\lambda_1) - [a_{ph}(\lambda_2) + a_y(\lambda_2) + a_w(\lambda_2) + b_b(\lambda_2)]/b_b(\lambda_2)\} * \{b_b(\lambda_3)/[a_{ph}(\lambda_3) + a_y(\lambda_3) + a_w(\lambda_3) + b_b(\lambda_3)]\} \quad (11)$$

Assuming $b_b(\lambda_1) \approx b_b(\lambda_2) \approx b_b(\lambda_3)$ and the dominance of $a_w(\lambda_3)$ over other terms at λ_3

$$[Chl] = \{[a_w(\lambda_3)R3 - a_w(\lambda_1) + a_w(\lambda_2)] + [a_y(\lambda_2) - a_y(\lambda_1)] + [b_b(\lambda_2) - b_b(\lambda_1)]\}/[a^*_{ph}(\lambda_1) - a^*_{ph}(\lambda_2)] \quad (12)$$

Despite the assumption about $b_b(\lambda)$, the term $[b_b(\lambda_2) - b_b(\lambda_1)]$ in (12) is left as non-zero in order to estimate possible errors. The contributions of all components to the relationship between [Chl] and R3 is shown in Fig. 7. [Chl] vs. R3 relationship is mostly defined by the water absorption term, with minimal effect of other components, which, as expected, is even smaller than that for the $R_{rs}(708)/R_{rs}(665)$ model because CDOM absorption term and backscattering term do not have R3 as a multiplier in the equation. The slope of the relationship is determined by the $a^*_{ph}(665)$ value in the denominator of Eq. (12).

#134029 - $15.00 USD Received 25 Aug 2010; revised 25 Oct 2010; accepted 26 Oct 2010; published 3 Nov 2010

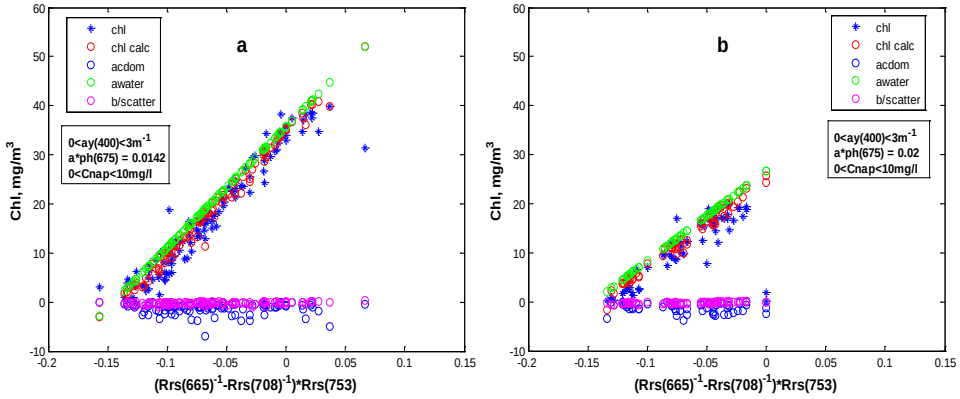

Fig. 7. Contributions of main components of Eq. (12) to the [Chl] vs R3 relationship: a) $a^*_{ph}(675) = 0.0142$ m^2/(mg Chl a), b) $a^*_{ph}(675) = 0.0142$ m^2/(mg Chl a). "chl" is the [Chl] from the data set, "chl calc" is the [Chl] from the Eq. (12), "acdom" is $[a_y(\lambda_2) - a_y(\lambda_1)] / a^*_{ph}(\lambda_2)$, the CDOM absorption term from (12), "awater" is $[a_w(\lambda_3)R3 - a_w(\lambda_1) + a_w(\lambda_2)] / a^*_{ph}(\lambda_2)$, the water absorption term from (12) and "b/scatter" is $[b_b(\lambda_2) - b_b(\lambda_1)] / a^*_{ph}(\lambda_2)$, the backscattering term from (12). The ranges of values for [Chl], a_y, and C_{NAP} are the same as for Fig. 5.

5. Relationship between [Chl] and phytoplankton specific absorption coefficient

The results derived from the simulated reflectance spectra show that the performance of the red - NIR models is strongly affected by the magnitude and spectral shape of the phytoplankton specific absorption coefficient. As it was already mentioned, a^*_{ph} decreases with increasing [Chl], especially for [Chl] > 3-5 mg/m^3, due to the packaging effect [27]. This decrease was observed for the mean value as well as the variability of a^*_{ph} [27], but the exact range of this decrease was not well studied, especially for [Chl] > 10 mg/m^3.

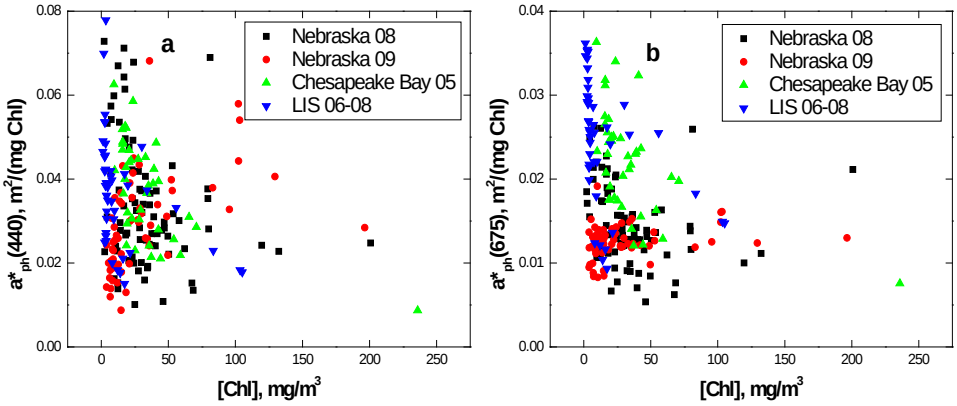

Fig. 8. Phytoplankton specific absorption coefficient at (a) 440 nm and (b) 675 nm plotted against [Chl] for the field data collected from inland and coastal waters.

Figure 8 shows the range of values for the peaks of a^*_{ph} at 440 and 675 nm in the data sets from several field campaigns [21,28,32] (the data from the Nebraska campaign in 2009 are

#134029 - $15.00 USD Received 25 Aug 2010; revised 25 Oct 2010; accepted 26 Oct 2010; published 3 Nov 2010

unpublished as yet). [Chl] values were obtained using standard measurement techniques [21,28]. Phytoplankton absorption values for Nebraska lakes were obtained using standard filter absorption measurements [28]. For the Chesapeake Bay and the Long Island Sound phytoplankton absorption spectra were retrieved from the total absorption spectra measured by an ac-s instrument (WET Labs) [32]. The variability of both $a^*_{ph}(440)$ and $a^*_{ph}(675)$, as shown in Fig. 8, is higher than those in [27]. Moreover, the mean values do not decrease with [Chl] as rapidly as reported in [27].

The power fit for $a^*_{ph}(675)$ vs. [Chl] for all points of Fig. 8(b) is shown in Fig. 9(a) (red solid line). The power equation is:

$$a^*_{ph}(675) = 0.03\,[Chl]^{-0.2} \tag{13}$$

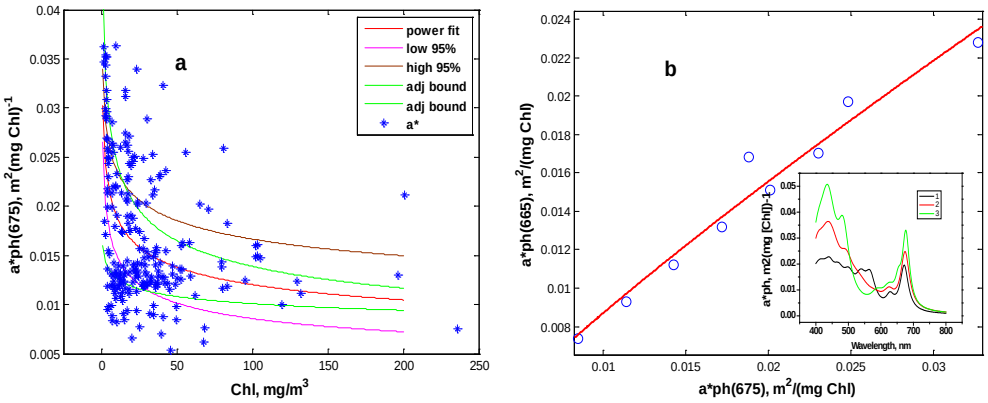

Fig. 9. a) power fit for all points of Fig. 8(b) for $a^*_{ph}(675)$ vs. [Chl]; $R^2 = 0.2265$; the brown and pink lines represent bounds for the 95% confidence interval. b) power fit for $a^*_{ph}(675)$ vs. $a^*_{ph}(665)$; $R^2 = 0.965$. Inset: a^*_{ph} spectra with higher $a^*_{ph}(675)$ values – specific absorption coefficient spectra of: Cryptophyta "H" (1), Diatoms (2) and Green algae (3) from Gege et al. [33].

The brown and pink lines in Fig. 9(a) represent the bounds for the 95% confidence interval. Taking into account the known decrease of variability in $a^*_{ph}(675)$ as [Chl] increases, we also added other bounds (green lines) with a wider range of $a^*_{ph}(675)$ values at low [Chl] (close to 1 mg/m^3) and a narrower range for higher [Chl]. These bounds were, for [Chl] = 1 mg/m^3, $a^*_{ph\ (max)}(675) = 0.0439$ m^2/(mg Chl a) and $a^*_{ph\ (min)}(675) = 0.016$ m^2/(mg Chl a) respectively. $a^*_{ph}(665)$ is always smaller than $a^*_{ph}(675)$ and it does not change proportionally with $a^*_{ph}(675)$. The relationship between $a^*_{ph}(665)$ and $a^*_{ph}(675)$ is shown in Fig. 9(b) and is approximated as

$$a^*_{ph}(665) = 0.412\ a^*_{ph}(675)]^{0.8373} \tag{14}$$

and together with (13)

$$a^*_{ph}(665) = 0.022\,[Chl]^{-0.1675} \tag{15}$$

The points in Fig. 9(b) are taken from the specific absorption coefficient spectra in Fig. 1 as well as from the spectra with higher a^*_{ph} values: these are spectra of Cryptophyta "H" (1), Diatoms (2) and Green algae (3) from Gege et al. [33], and are shown in the inset of Fig. 9(b).

#134029 - $15.00 USD Received 25 Aug 2010; revised 25 Oct 2010; accepted 26 Oct 2010; published 3 Nov 2010

Analysis of $a^*_{ph}(675)$ as a function of [Chl] shows that $a^*_{ph}(675)$ values in the inland and coastal waters studied are in the range of 0.02 – 0.03 m^2/(mg Chl) for [Chl] ≈1mg/m^3 and gradually decreases to 0.01 – 0.015 m^2/(mg Chl) for [Chl] > 10-20 mg/m^3. Spectra in Fig. 1 give lower values of $a^*_{ph}(675)$ especially for [Chl] < 10-20 mg/m^3, which makes simulations less accurate. Additional measurements for various water conditions are necessary for the clarification of this issue.

6. Advanced versions of two- and three-band models and their comparison with the field data

Based on the conclusion in Section 4, water absorption terms are dominant in the equations for the two-band model, $R_{rs}(708)/R_{rs}(665)$ [Eq. (9)] and the three-band model, $[R_{rs}(665)^{-1} – R_{rs}(708)^{-1}]*R_{rs}(753)$ [Eq. (12)]. So Eq. (9) can be simplified as

$$[\text{Chl}] = [a_w(\lambda_1)R2 - a_w(\lambda_2)] / a^*_{ph}(665) \tag{16}$$

Then substituting $a^*_{ph}(665)$ from Eq. (15) after simple modifications, we arrive at

$$[\text{Chl}] = \{[a_w(\lambda_1)R2 - a_w(\lambda_2)] / 0.022\}^{1/p} \tag{17.1}$$

$$[\text{Chl}] = [35.75 * R2 - 19.30\ ]^{1.124} \tag{17.2}$$

Similarly, for the three-band model, Eq. (12) can be simplified as,

$$[\text{Chl}] = [a_w(\lambda_3)R3 - a_w(\lambda_1) + a_w(\lambda_2)] / a^*_{ph}(665) \tag{18}$$

and after including $a^*_{ph}(665)$ from Eq. (15),

$$[\text{Chl}] = \{[a_w(\lambda_3)R3 - a_w(\lambda_1) + a_w(\lambda_2)] / 0.022\}^{(1/p)} \tag{19.1}$$

$$[\text{Chl}] = [113.36 * R3 + 16.45\ ]^{1.124} \tag{19.2}$$

For both Eqs. (17.1) and (19.1), p = 0.8325. In order to better fit the field data, p was adjusted slightly from 0.8325 to 0.89. Comparison of relationships Eqs. (17.1) and (19.1) with the Nebraska field data for all three models is shown in Fig. 10. Respective values in the power coefficient for the upper and lower bounds corresponding to the bounds in Fig. 9(a) were also increased accordingly by δ = [0.89 – 0.8325] = 0.0575.

Taking $a_w(665)$ = 0.4245 m^{-1}, $a_w(708)$ = 0.7864 m^{-1}, and $a_w(753)$ = 2.494 m^{-1} ([31] with interpolation), Eqs. (17.1) and (19.1) with p = 0.89 can be rewritten as Eqs. (17.2) and (19.2), where $R2 = R_{rs}(708)/R_{rs}(665)$ and $R3 = (1/R_{rs}(665) – 1/R_{rs}(708))*R_{rs}(753)$.

Very close relationships between the field data [28] and both the two-band model, $R_{rs}(708)/R_{rs}(665)$, and the three-band model, $[R_{rs}(665)^{-1} – R_{rs}(708)^{-1}]*R_{rs}(753)$ are observed in Fig. 10. Once again, the two-band model, $R_{rs}(753)/R_{rs}(665)$, proved to be inaccurate for low to moderate [Chl]. MERIS-derived relationships for the $R_{rs}(708)/R_{rs}(665)$ model, and the three-band model [Eqs. (3) and (4) respectively] from Moses et al. [29] [cyan lines in Fig. 10(a) and Fig. 10(c)] match very well with the linear parts of the analytically derived algorithms, Eqs. (17.2) and (19.2) [red lines in Fig. 10(a) and 10(c)]. Equations (17.2) and (19.2) match well with the field data even in the non-linear part of the curve for [Chl] < 10mg/m^3. Correlations between measured [Chl] from the Nebraska field data set and [Chl] from the analytically derived algorithms for the models $R_{rs}(708)/R_{rs}(665)$ [Eq. (17.2) and $[R_{rs}(665)^{-1} – R_{rs}(708)^{-1}]*$ $R_{rs}(753)$ (Eq. (19.2)] are shown in Fig. 11. In both cases, the determination coefficient is above 0.95.

#134029 - $15.00 USD Received 25 Aug 2010; revised 25 Oct 2010; accepted 26 Oct 2010; published 3 Nov 2010

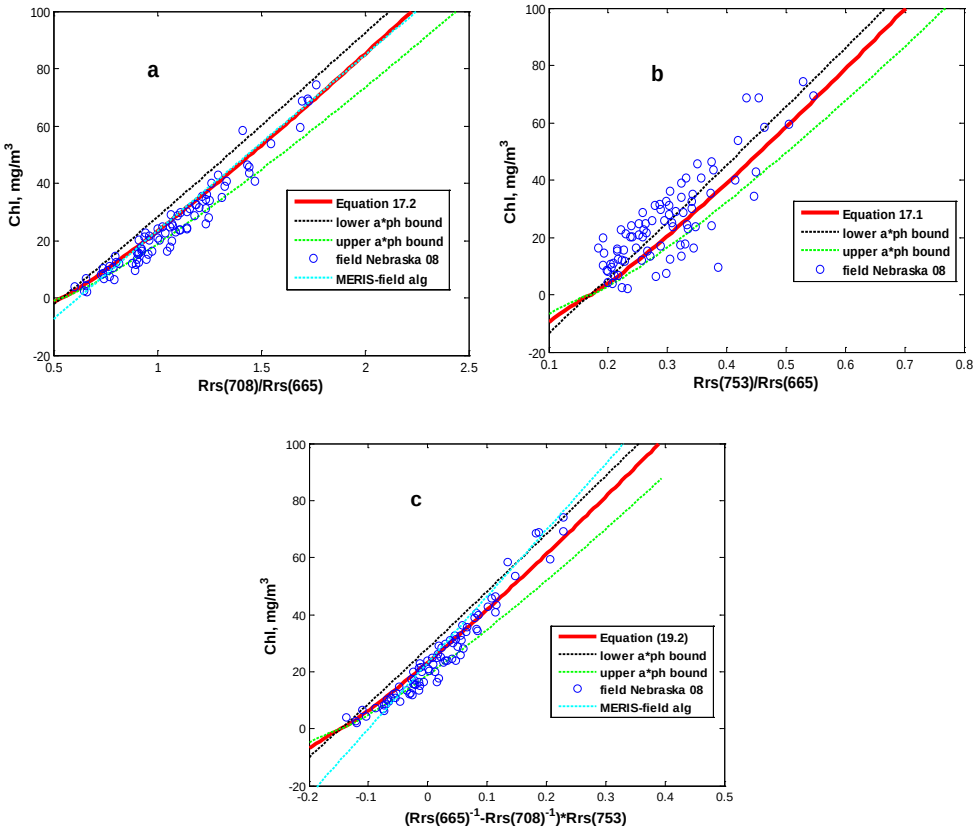

Fig. 10. Comparison of analytical relationships Eqs. (17.1) and (19.1) with the field data (Nebraska 2008 [28]) and empirical algorithms from MERIS –field data [29]: a) R2: Rrs(708)/Rrs(665), b) R2: Rrs(753)/Rrs(665), c) R3 = $[Rrs(665)^{-1} – Rrs(708)^{-1}]$*Rrs(753). Red lines correspond to the Eq. (17.1) and (17.2) for Rrs(708)/Rrs(665) algorithm [Fig. 10(a)], the Eq. (17.1) for Rrs(753)/Rrs(665) algorithm [Fig. 10(b)] and to the Eqs. (19.1) and (19.2) for $[Rrs(665)^{-1} – Rrs(708)^{-1}]$ *Rrs(753) algorithm [Fig. 10(c)]. Lower and upper a^*_{ph} bounds correspond to the bounds in Fig. 9(a), MERIS – field algorithm – cyan lines [Eq. (3)] for Rrs(708)/Rrs(665) algorithm [Fig. 10(a)] and Eq. (4) for 3 bands algorithm [Fig. 10(c)].

It should be also noted that $a^*_{ph}(675)$ decreases rapidly with [Chl] below 5-10 mg/m^3 [Fig. 9(a)], but in this [Chl] range its impact on the algorithms is minimal (see Fig. 3). For higher [Chl] values, the $a^*_{ph}(675)$ change is much smaller as is its impact on the algorithms. For the whole [Chl] range the impact is also mitigated by the fact that the algorithms use $a^*_{ph}(665)$ which, according to Eq. (14), has much weaker dependence on [Chl] than $a^*_{ph}(675)$. As a result, a very broad range of $a^*_{ph}(675)$ in Fig. 9(a) (upper bound was approximated as $0.0439[Chl]^{-0.25}$ and lower bound as $0.016[Chl]^{-0.1}$) corresponds to a relatively small range of [Chl] variations between lower and upper boundaries [Fig. 10(a) and 10(c)], which makes both two- and three-bands algorithms less sensitive to changes in the phytoplankton specific absorption.

#134029 - $15.00 USD Received 25 Aug 2010; revised 25 Oct 2010; accepted 26 Oct 2010; published 3 Nov 2010

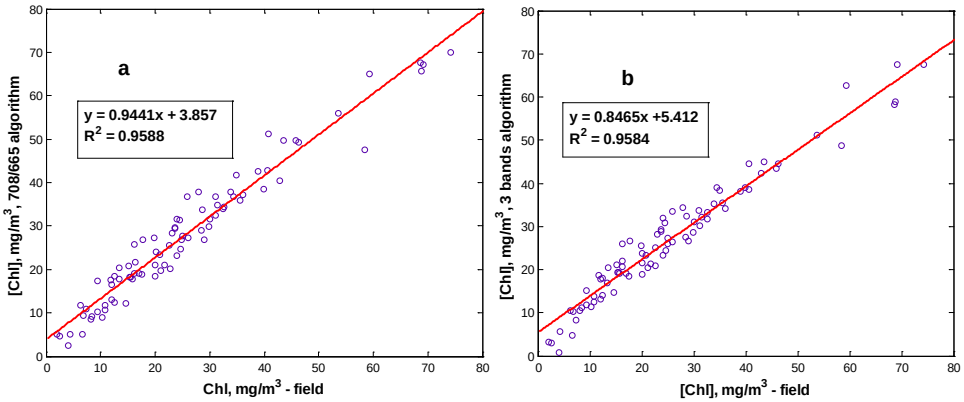

Fig. 11. Correlations between [Chl] measured in the Nebraska and [Chl] from the analytically-derived [Chl] from (a) Eq. (17.2): Rrs(708)/Rrs(665), and (b) Eq. (19.2): $[Rrs(665)^{-1} - Rrs(708)^{-1}]*Rrs(753)$.

Additional studies in various water conditions and water environments are necessary for the estimation of the actual sensitivity of the models to a^*_{ph}. In such investigations special attention should be given to the accuracy of [Chl] and a^*_{ph} measurements.

7. Comparison of the performance of the blue-green MODIS OC3M and red/NIR algorithms

We also analyzed the performance of the blue-green MODIS OC3M algorithm [34] using the same data sets to compare it with the red–NIR algorithms. Higher variability of $a^*_{ph}(440)$ observed in the field [Fig. 8(a)] corresponds to a broad range of a^*_{ph} with S_f in the range 0-0.6. Preliminary estimations showed that S_f in the range 0-0.2 can be used for the assessment of OC3M for the whole range of [Chl] = 1-100 mg/m^3. Higher S_f values are valid for [Chl] < 10-20 mg/m^3 and these results are not presented below.

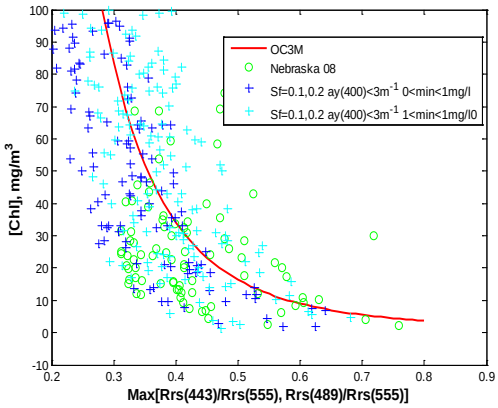

Fig. 12. Performance of OC3M algorithm on synthetic and field data. On the x-axis is the blue-green ratio, which is the primary element of the OC3M algorithm. The red curve represents the [Chl] values estimated by the OC3M algorithm.

In Fig. 12 we show the relationship between [Chl] and the maximum of two ratios, R_{bg} = Max[$R_{rs}(443)/R_{rs}(555)$, $R_{rs}(489)/R_{rs}(555)$], which is the primary element of the OC3M algorithm. The solid red line shows [Chl] values estimated from the R_{bg} ratios based on the

#134029 - $15.00 USD Received 25 Aug 2010; revised 25 Oct 2010; accepted 26 Oct 2010; published 3 Nov 2010

OC3M algorithm. The field data and synthetic data are both distributed approximately the same way along the OC3M line but the spread is quite high for both data sets.

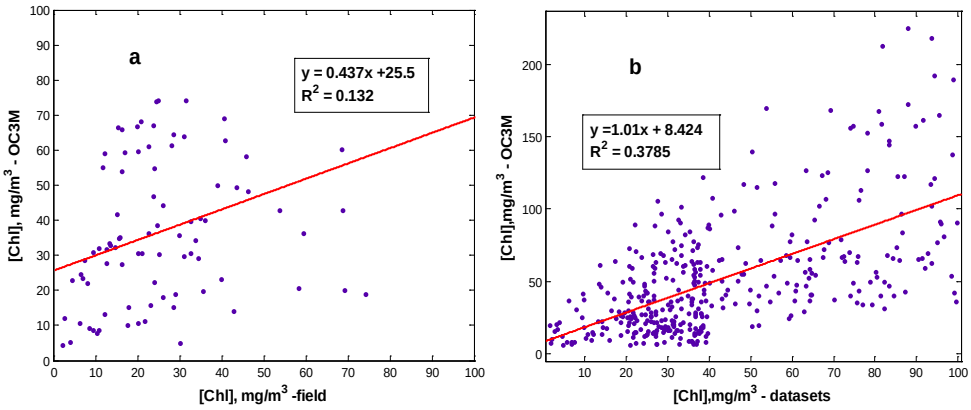

Fig. 13. Plots of OC3M-derived [Chl] versus (a) [Chl] from the Nebraska field data set and (b) synthetically derived [Chl]. Concentrations of non-algal particles, C_{NAP}, ranged from 0 to 10 mg/l, CDOM absorption was in the range of $0<a_y(400)<3$ m^{-1}.

Correlation between the field measured [Chl] and the blue-green algorithm [Chl] [Fig. 13(a)] and the correlation between the synthetic [Chl] and the blue-green algorithm [Chl] [Fig. 13(b)] are significantly lower (R^2 is below 0.4) than those for the red – NIR algorithms. Thus, for estimating [Chl] > 3-5g/m^3, the red-NIR algorithms are significantly more accurate than the blue-green algorithm.

8. Conclusions

Several synthetic data sets of reflectances and inherent optical properties simulated with Hydrolight for inland and coastal waters and a very consistent field data set with [Chl] = 2 –100 mg/m^3 were utilized to evaluate (a) the performance of red-NIR algorithms for the remote estimation of chlorophyll-a concentration and (b) the sensitivity of these algorithms to the main water parameters that characterize the optical properties of water, namely, absorption and backscattering coefficients. Two-band algorithms under study were $R_{rs}(708)/R_{rs}(665)$ and $R_{rs}(753)/R_{rs}(665)$. The three-band algorithm was $[1/R_{rs}(665) – 1/R_{rs}(708)]*R_{rs}(753)$. All algorithms use wavebands that match the MERIS spectral channels. The main results and conclusions are the following.

1. The red-NIR algorithms are affected by possible variations in phytoplankton specific absorption coefficient in the red – NIR part of the spectrum. The realistic ranges of $a^*_{ph}(675)$ and $a^*_{ph}(665)$ and their dependence on [Chl] for various water environments were determined based on the experimental data taken in coastal and inland waters and absorption spectra analysis. It is shown that both mean values and variability of values do decrease with increase in [Chl] but more gradually than presented in [27]. It is also shown that the red-NIR algorithms are not very sensitive to the phytoplankton specific absorption coefficient because the most rapid change in $a^*_{ph}(665)$ in response to a change in [Chl] occurs at [Chl] < 5-10 mg/m^3, where its impact on the algorithms is minimal.

2. The contributions of CDOM and water absorption and particulate backscattering in the basic relationships for the red – NIR algorithms were evaluated using synthetic data sets. The $R_{rs}(708)/R_{rs}(665)$ model and the three-band model are not very sensitive to CDOM absorption and backscattering by non-algal particles and the model equations are mostly controlled by terms that contain water absorption coefficients as well as by phytoplankton specific absorption coefficients. It was also shown that chlorophyll fluorescence does not noticeably affect the performance of these models. On the contrary, the $R_{rs}(753)/R_{rs}(665)$ model

#134029 - $15.00 USD Received 25 Aug 2010; revised 25 Oct 2010; accepted 26 Oct 2010; published 3 Nov 2010

appeared to be very sensitive to the main water optical properties and cannot be used for estimating low to moderate [Chl].

3. Established a_{ph}*(665) vs. [Chl] relationship and the simplified basic equations were used for the analytical development of advanced versions of $R_{rs}(708)/R_{rs}(665)$ and $[1/R_{rs}(665) - 1/R_{rs}(708)]*R_{rs}(753)$ algorithms, whose [Chl] estimations matched very well with the field data even for [Chl] < 10mg/m^3. The analytically derived algorithms also matched well with red-NIR algorithms that were previously calibrated using MERIS data [29]. This suggests that these algorithms, which are based on the known values of the water absorption coefficient at the appropriate bands and generalized a_{ph}*(665) vs. [Chl] relationship, do not require regional tuning.

4. It is shown that the performance of the blue-green ratio based algorithm is poor in turbid productive inland and coastal waters and that the red-NIR algorithms are much preferred for these waters.

Future work will include validation of the developed algorithms for water bodies from various regions, with an emphasis on the study of the variation of the a_{ph}*(665) vs. [Chl] relationship.

Acknowledgements

This work has been supported by grants from National Oceanic and Atmospheric Administration (NOAA), the Office of Naval Research (CCNY group), and the National Aviation and Space Administration (NASA) Land-Cover/Land – Use Change Program, and by the University of Nebraska Agricultural Research Division, Lincoln (CALMIT group). We would like to thank Dr. Z. P. Lee and two other anonymous reviewers for their comments and suggestions which helped to improve the manuscript.

#134029 - $15.00 USD Received 25 Aug 2010; revised 25 Oct 2010; accepted 26 Oct 2010; published 3 Nov 2010